DOI 10.5162/sensor2017/B5.4

Low-coherence Interferometry for Industrial Applications

Johann Krauter, Tobias Boettcher, Marc Gronle, Wolfgang Osten
Institut für Technische Optik, University Stuttgart, Stuttgart, 70569, Germany
krauter@ito.uni-stuttgart.de

Abstract

Today, micro-electro-mechanical systems (MEMS) are found in various devices and different industries such as automotive, multimedia or medicine. It is desirable to have a 100 % performance test of each individual MEMS before more than 90 % of the production costs is incurred during the dicing, bonding and packaging procedures. Prior to these steps, all MEMS are subjected to an electrical test. We demonstrate an adapted low-coherence interferometer (LCI), that is suitable for the inspection of those MEMS structures located below the silicon cap. First LCI wavelets are shown, which are used to calculate the topography of the MEMS. Another challenging aspect of modern metrology techniques is their application for in-line inspection. Therefore, another new interferometer approach is presented in the second part of this paper, which provides a very robust, single-shot acquisition of one point with the possibility to be extended to a single-shot line acquisition.

Keywords: low-coherence interferometry, MEMS, topography metrology, mirror optics, SWIR

Introduction

Since the 2000s, the MEMS industry has grown almost exponentially due to the demand of the consumer market [1]. The basic production process is a repeated combination of layer deposition, lithographically patterning of the photoresist and etching of the underlying materials until all structures are created [2]. For protection, a silicon cap is bonded to the MEMS wafer. An electrical test is applied to each MEMS. In case of a failed test, it is not possible to identify and localize possible defects on the structures since they are no longer accessible for optical inspection. An optical inspection would be desirable prior to the dicing, bonding and packaging procedure because 90 % of the costs arise during these steps. The dimension of the MEMS structures is typically in the micrometer range, meaning that an optical inspection system with high resolution in the axial and lateral direction is unavoidable. We demonstrate a low-coherence interferometer, whose base concept is well known in the field of high accuracy measurements [3], for the inspection of those MEMS structures through the silicon cap. The MEMS topography is calculated by the evaluation of the detected interferograms to identify defects, like bent MEMS fingers. In the next chapter, this setup is presented in detail.

A typical MEMS production line produces several million individual MEMS parts per day. This means that only sensors can be applied here, that allow very fast inspection. Under these circumstances, the typical scanning inspection sensors are very unattractive. In a second chapter, a new interferometric approach is shown, which is suitable for a fast in-line inspection.

Interferometric measurement of hidden MEMS

Various techniques for the inspection of microsystems are known in optical metrology [3]. For instance, fringe projection can be used for a topographic measurement of “large” objects [4], but it is limited to scattering surfaces and has a resolution in the micrometer range. Confocal microscopy is suitable for multilayer objects, where the confocal filtering separates each object layer. The axial resolution is typically in the micrometer range and is limited by the numerical aperture (NA) of the objective lens (MO) [5]. A resolution in the sub-wavelength range is achieved with interferometric techniques. For topographic measurements, the scanning white-light interferometry (SWLI) is state of the art [6]. In comparison, the optical coherence tomography (OCT) is used for low scattering multilayer objects, that are common in biomedicine [7]. Digital holography [8] or vibrometry [9] are used to measure the dynamic properties of MEMS.

Interferometer setup

The objective of this setup is to measure the topography of the MEMS, which are located inside the wafer-stack as shown in fig. 1. It should be possible to identify sticky or bend MEMS by the topography measurement. The structures within the wafer stack can be observed through the silicon cap on top or through the MEMS-wafer at the bottom of the wafer stack. However, the accessibility through the top is sometimes limited by additional

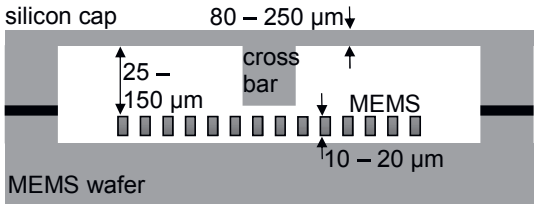

Fig. 1. Cross-section of the MEMS wafer-stack.

reinforcement structures, like the depicted cross-bar at the bottom surface of the silicon cap wafer. The structural dimensions are in the micrometer range such that a MO with a high NA is necessary. The typical Michelson interferometer MO [6] is limited to low NA due to the beamsplitter in front of the MO. A Mirau MO cannot be used for the imaging through variable slab thicknesses because the matched path lengths are not variable. An interferometric setup with high NA with variable path lengths is only possible in the Linnik configuration as shown in fig. 2 [10]. The applied wavelength has to be in the short-wavelength infrared (SWIR) above 1.1 µm where silicon becomes transparent [11]. The setup is illuminated via a superluminescent diode (SLD) at a center wavelength of 1.55 µm, a spectral width of 70 nm and an optical power of 12 mW. The temporal coherence length limits the axial resolution, which is approximately 15.15 µm. At this wavelength, the refractive index n_{Si} of silicon is 3.48 [11]. The reflection of a silicon surface is about 30 % due to the Fresnel reflection [12]. Without further loss, the intensity, which is reflected by the top MEMS surface to the camera is about 7 %. A two-beamsplitter arrangement has been used to match the object and reference intensity without losing light as it is typically done by reducing the reference mirror reflectivity. Two Olympus LCPLN50XIR MO with a NA of 0.65 are aligned in the Linnik configuration [13]. According to the Rayleigh criterion the lateral resolution is 1.4 µm. By focusing through a slab of dielectric of thickness t, spherical aberration occurs, because the marginal rays have a longer optical path than the chief ray. This slab introduces a phase error, which can be expressed by [14]:

$$\phi_{max} = \frac{kt}{2}(n_2^2 - n_1^2)\frac{n_1^2}{n_2^3}\sin^4\left(\frac{\alpha}{2}\right), \qquad (1)$$

where k is the wavenumber, n_1 is the refractive index of air and α the semi-angle of convergence. A silicon cap thickness of 100 µm introduces a phase error of 0.12 λ by focusing with a NA of 0.65. Given a telecentric MO, the spherical aberrations are constant over the field since the chief ray of each field point propagates perpendicular to the slab. In general, an adapted tube lens corrects spherical aberration of a microscope [15]. In this setup, a flexible correction is needed, because each MEMS type has a different cap-wafer with other thicknesses t. The used MO has a correction mechanics for spherical aberration induced by slabs with a thickness of up to 1.2 mm of glass or silicon. A tube lens with 100 mm focal length images the superposition of the reference and object onto the infrared InGaAs camera with 640x512 pixel and a pitch of 15 µm [16]. The interferogram is acquired by an axial scan of the reference path, which is realized by the piezo actuator PI PIFOC P-725.2 CD, which has a closed-loop resolution of 0.75 nm [17].

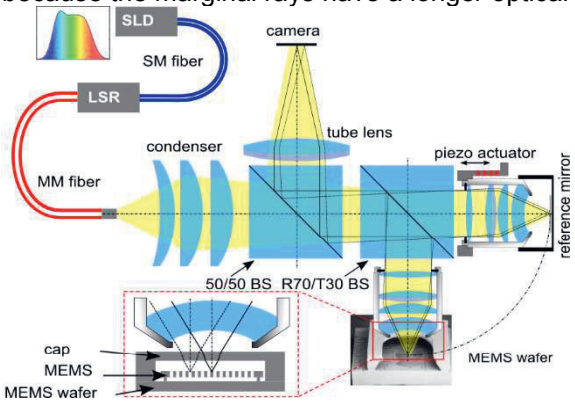

Fig. 2. Concept of the interferometer [27]

First measurements

In [18] first topography and tomography measurement were shown without any further discussion. In the following, first topography measurement results measured by the reported setup are presented. Fig. 3 shows one exemplary detected wavelet, which was reflected at the MEMS surface. In [19], [20] is it shown that the full width at half maximum (FWHM) of the wavelet envelope increases due to dispersion effects. Here the calculated FWHM is 16.23 µm and thus slightly larger than the theoretical one. In this measurement, the dispersion effect is not as high as in the visible spectrum, because the slope $\Delta n/\Delta\lambda$ of the dispersion curve of silicon reduces with increasing wavelengths. Calculated from the

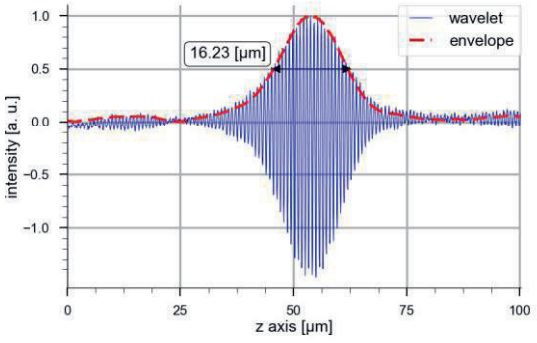

Fig. 3. Detected wavelet of one camera pixel.

Sellmeier equation of silicon [21], [22], the dispersion slope $\Delta n/\Delta\lambda$ for NIR is $\Delta n/\Delta\lambda_{@850}$ = -0.57 10^{-3} 1/nm. In the SWIR the slope is much flatter with $\Delta n/\Delta\lambda_{@1550nm}$ = -8.2 10^{-5} 1/nm.

Fig. 4 shows two height maps after the evaluation of the interferometric signal by the lock-in algorithm [23], [24]. Here wavelets with a low interferometric contrast and bad camera pixel are not evaluated. These pixels are filled with interpolated height values just for better visualization. In fig. 4 (a) the MEMS where imaged through the cap-wafer. From this direction it is not, possible to measure the topography of the MEMS above the cross bar, because the distance here is less than the axial resolution.

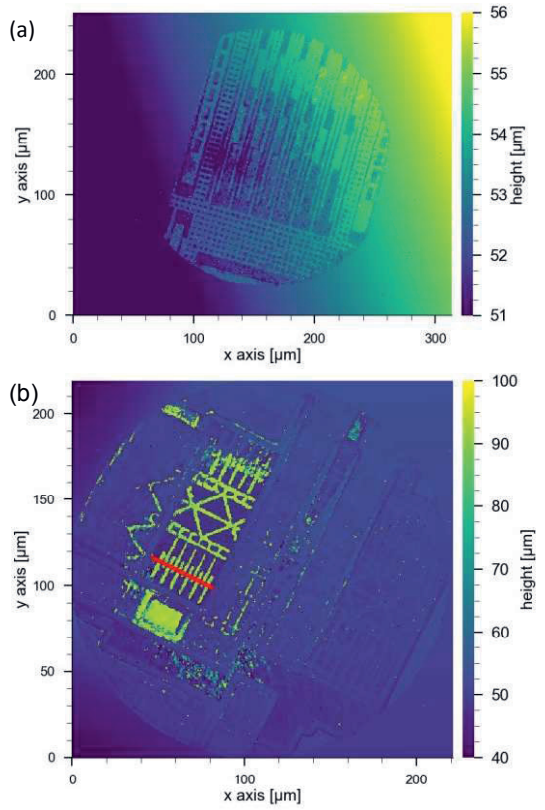

Fig. 4. (a) Measurement through the cap wafer. (b) Measurement through the MEMS-wafer.

The height map in fig. 4 (b) was performed through the bottom MEMS-wafer. However, some parts of the structures can also not be resolved due to some electrical conductor tracks that are located on the bottom wafer. On the left side of the field, there are no tracks where the MEMS are clearly visible. In the background of the MEMS is the silicon cross bar. A cross-section along the marked red line is shown in fig. 5. Here the lateral structure of the MEMS fingers is resolved with a width of about 1.9 µm. At the lower level is the cross bar surface located and at the top level at a distance of about 45 µm is the surface of the MEMS.

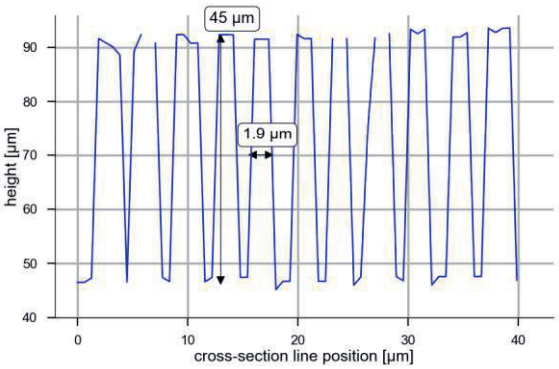

Fig. 5. Cross-section along the red line of fig. 5.

LCI approach for in-line inspection

The conventional scanning optical measurement systems are very unattractive for an in-line inspection. Here single-shot sensors are required, which have a significantly low measurement time. We want to show a new type of single-shot LCI sensor [24], [25]. The principle idea is to detect the interference of two tilted wavefronts. The tilt of the reference wavefront is introduced by a mirror arrangement of three faceted mirror surfaces (TFM) as illustrated in fig. 6.

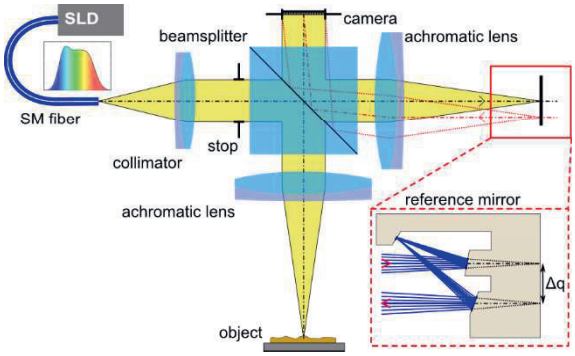

Fig. 6. Concept of the single-shot LCI [24].

The focused ray bundle in the reference is reflected with a lateral shear, resulting in a tilted wavefront in the back focal plane of the achromatic objective lens. At this position and under the consideration of a broadband spectrum, a low-coherence interferogram is detected just by one camera frame. The lateral shear is calculated by:

$$\Delta q = f \times \tan\left(\sin^{-1}\frac{\lambda_0}{h}\right). \qquad (2)$$

In this setup, a shear Δq of 1.54 µm has been chosen to guarantee a sampling of 10 pixel/fringe period with a center wavelength λ_0 of 850 nm and a spectral width $\Delta\lambda$ of 40 nm. For the first demonstration, a focal length f of 100 mm has been chosen. The fringe period h on the camera is calculated by:

$$h = \frac{\lambda_0}{\sin\alpha}, \qquad (3)$$

with the tilt angle α at the camera position. Fig. 7 shows the detected interferogram of one camera pixel line.

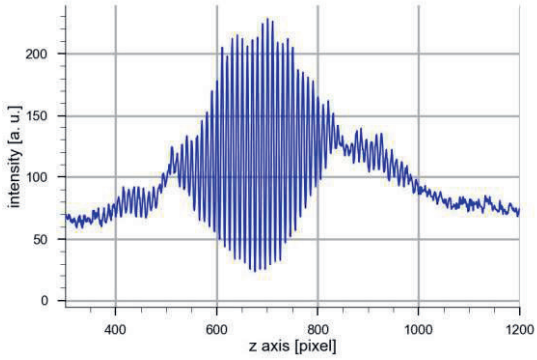

Fig. 7. Signal of one camera pixel line

This first laboratory setup is a point-scanning single-shot sensor. For a demonstration of the feasibility, it has been used to scan over the Halle depth calibration standard. The lock-in algorithm was used for the evaluation of the interferograms [23], [24]. Fig. 8 presents the height profile of this measurement where the groove depths are resolved. Each groove depth is calculated between interpolated height level values.

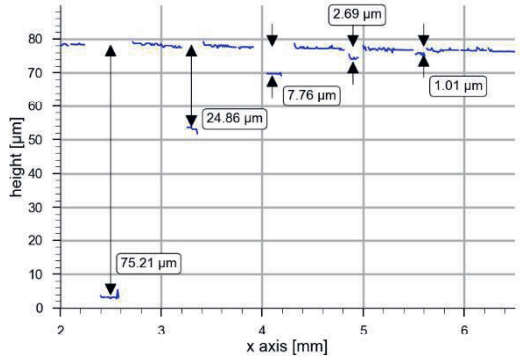

Fig. 8. Measurement of the depth calibration standard [20].

The reference mirror has been designed with rectangular surfaces to further extend the sensor to a line-wise single-shot LCI sensor. If the achromatic lenses are replaced by achromatic cylindrical lenses, the interference signal of different points along the line is spread over all rows of the entire camera frame. The layout of a Zemax simulation illustrates the reference path with a cylindrical lens and the TFM in fig. 9. A simulation of the expected camera image was performed by using itom [26] and the Zemax ZOS-API interface. For the demonstration of different object heights, the object mirror has a slight tilt. Fig. 10 a shows the resulting camera image. Along the y-axis, the position of the wavelet changes due to the tilted object mirror. Line 1 and line 2 are two extracted cross-section

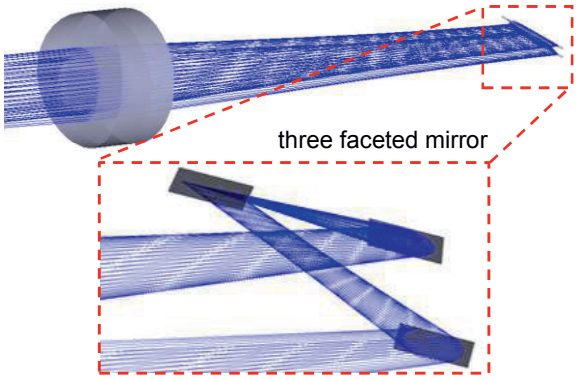

Fig. 9. Zemax 3D layout of the reference mirror and an achromatic cylindrical lens.

lines (fig. 10(b)). Each one has a wavelet at a different x-axis position. After the signal evaluation of each wavelet, the tilt of the object mirror can be reconstructed (marked in red).

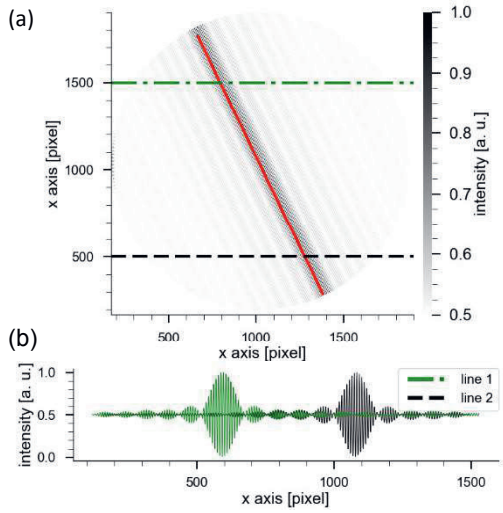

Fig. 10. (a) Simulated camera image with a different interferogram in each camera line corresponding to different object heights. (b) Two cross-sections through the camera image with various positions of the interferogram.

Conclusion

In this paper, a low-coherence interferometer for the optical topography measurement of MEMS structures located under the silicon cap was shown. Since silicon becomes transparent in the infrared, the setup must operate at a wavelength above 1.1 µm. First topography measurements were shown, which were acquired by a scanning low-coherence interferometer. The lateral structure of 2 µm of the MEMS was resolved by the high numerical microscope objective lens in a Linnik interferometer. The topography of the MEMS was reconstructed by the evaluation of the low-coherence wavelets.

In addition, a second interferometric setup was described. This setup allows a single-shot acquisition of low-coherence wavelets, what makes it very attractive for inspection task in the

production like the fabrication of MEMS devices. Its key component is a three faceted mirror, which reflects a focused beam with a lateral shear, resulting in a tilted wavefront at the camera position and as a result a spatially modulated interferogram. First height measurements of the Halle depth calibration standard demonstrate the feasibility of the sensor. A simulation further shows, that this sensor can be adapted to a line-wise single-shot low-coherence interferometer sensor, where the line is encoded in the one axis of the camera and every interferogram is created along the second axis.

References

[1] V. Lindroos, M. Tilli, A. Lehto, and T. Motooka, Handbook of silicon based MEMS materials and Technologies, Oxford: Elsevier Science & Technology (2010)

[2] N. Maluf and K. Williams, An Introduction to Microelectro-mechanical Systems Engineering, 2nd ed. Boston, London: Artech House, Inc. (2004)

[3] W. Osten, Optical inspection of microsystems, Boca Raton: CRC Press (2007)

[4] K. Leonhardt, U. Droste, and H. J. Tiziani, Microshape and rough-surface analysis by fringe projection, *Appl. Opt.* 33, 31 (1994); doi: 10.1364/AO.33.007477

[5] T. Wilson, Confocal Miscroscopy, London: Academic Press (1990)

[6] G. S. Kino and S. S. C. Chim, Mirau correlation microscope, *Appl. Opt*. 29, 26 (1990); doi: 10.1364/AO.29.003775

[7] W. Drexler and J. G. Fujimoto, Optical Coherence Tomography. Berlin, Heidelberg: Springer Verlag (2008)

[8] A. Asundi, Digital Holography for MEMS and Microsystem Metrology. John Wiley & Sons, Ltd (2011)

[9] P. Krehl, S. Engemann, C. Rembe, and E. P. Hofer, High-speed visualization, a powerful diagnostic tool for microactuators - retrospect and prospect, *Microsyst. Technol.* 5, 1999 (1999); doi: 10.1007/s005420050151

[10] M. Davidson, K. Kaufman, I. Mazor, and F. Cohen, An application of interference microscopy to integrated circuit inspection and metrology, *in Proc. of SPIE* 0775 (1987); doi: 10.1117/12.940433

[11] M. A. Green and M. J. Keevers, Optical properties of intrinsic silicon at 300K, *Prog. Photovoltaics* 3, 3 (1995); doi: 10.1002/pip.4670030303

[12] E. Hecht, Optik, 4th ed. München: Oldenbourg Wissenschaftsverlag, (2002)

[13] Olympus GmbH, datasheet LMPLN-IR/LCPLN-IR, 2017, www.olympus-ims.com (2017)

[14] C. J. R. Sheppard and C. J. Cogswell, Effects of aberrating layers and tube length on confocal imaging properties, *Optik (Stuttgart)* 87, 1 (1991)

[15] C. J. R. Sheppard and M. Gu, Aberration compensation in confocal microscopy, *Appl. Opt*. 30, 25 (1991); doi: 10.1364/AO.30.003563

[16] New Imaging Technologies, datasheet Widy SWIR 640U-S, www.new-imaging-technologies.com (2017)

[17] Physikinstrumente GmbH, datasheet PIFOC P-725.2CD, www.physikinstrumente.de (2017)

[18] M. P. Saltmarsh, Failure Analysis Challenges of Surface Micromachined Accelerometers, *in ISTFA '97: Proceedings of the 23rd International Symposium for Testing and Failure Analysis* (1997)

[19] P. Pavlíček and J. Soubusta, Measurement of the influence of dispersion on white-light interferometry, *Appl. Opt.,* 43, 4, (2004); doi: 10.1364/AO.43.000766

[20] A. Pförtner and J. Schwider, Dispersion error in white-light linnik interferometers and its implications for evaluation procedures, *Appl. Opt.,* 40, 34 (2001); doi: 10.1364/AO.40.006223

[21] C. D. Salzberg and J. J. Villa, Infrared Refractive Indexes of Silicon Germanium and Modified Selenium Glass, *J. Opt. Soc. Am*., 47, 3 (1957); doi: 10.1364/JOSA.47.000244

[22] B. Tatian, Fitting refractive-index data with the Sellmeier dispersion formula, *Appl. Opt.,* 23, 24 (1984); doi: 10.1364/AO.23.004477

[23] M. Fleischer, R. Windecker, and H. J. Tiziani, Fast algorithms for data reduction in modern optical three-dimensional profile measurement systems with MMX technology, *Appl. Opt*. 39, 8 (2000); doi: 10.1364/AO.39.001290

[24] R. Hahn, J. Krauter, K. Körner, M. Gronle, and W. Osten, Single-shot low coherence pointwise measuring interferometer with potential for in-line inspection, *Meas. Sci. Technol*. 28, 2 (2017); doi: 10.1088/1361-6501/aa52f1

[25] K. Körner, R. Berger, and W. Osten, Method and arrangement for robust interferometry for detecting a feature of an object, *US 8,934,104 B2 Patent* (2015)

[26] M. Gronle, W. Lyda, M. Wilke, C. Kohler, and W. Osten, itom: an Open Source Metrology, Automation, and Data Evaluation Software, *Appl. Opt.* 53, 14 (2014); doi: 10.1364/AO.53.002974

[27] C. Johnson, Gyroscopes adding up to next commodity MEMS, www.memsjournal.com (2017)